Multimedia Tools and Applications
https://doi.org/10.1007/s11042-024-18994-3

Golden jackal optimization with lateral inhibition for image matching

Jinzhong Zhang[1] · Gang Zhang[1] · Min Kong[1] · Tan Zhang[1] · Duansong Wang[1]

Received: 19 October 2022 / Revised: 23 December 2023 / Accepted: 14 March 2024

Abstract
Image matching is a consequential branch of the discipline that integrates several theories and technologies, such as pattern recognition, image processing, computer vision and feature extraction. This investigation constructs a golden jackal optimization (GJO) established on lateral inhibition (LI) named LI-GJO to accomplish this issue. The stated intention is to execute a pixel-for-pixel comparison methodology to locate the appropriate portion of the template photograph in the original photograph and guarantee the matching precision by assessing the similarities or distinctions between the two photographs. The GJO, motivated by the jackal's synchronized foraging, exhibits its procedure of scavenging for prey, wrapping around prey and attacking prey to furnish the most appropriate solution. The GJO manipulates discovery and extraction to arrive at exceptional measured precision and prompt convergence productivity. The lateral inhibition preprocesses the original and template photographs to compensate for the visual information's loss, strengthen the gray gradient and spatial resolution, and upgrade the photograph matching precision. To ascertain the sustainability and adaptability, the LI-GJO has been contrasted with LI-AO, LI-DOA, LI-SHO, LI-SMA, LI-SOA, LI-STOA and LI-TSA. The experimental conclusions exhibit that the LI-GJO has substantial consistency and durability to prohibit precocious convergence and attain a higher anticipated precision, greater matching proficiency, better convergence effectiveness and stronger stability. The LI-GJO is an appropriate and practical methodology for addressing image matching.

Keywords Golden jackal optimization · Lateral inhibition · Image matching · Discovery and extraction · Experimental conclusions

1 Introduction

An influential branch of investigation that emerged from the amalgamation of a majority propositions and methodologies, which incorporates pattern identification and image manipulation, called image matching. The ambition is to navigate a pixel-for-pixel

✉ Gang Zhang
zhanggang@wxc.edu.cn

[1] School of Electrical and Optoelectronic Engineering, West Anhui University, Lu'an 237012, China

comparison methodology to locate the template photograph for the analogous spot in the original photograph and estimate if the reference photograph and the template photograph vary or are similar to accomplish the matching effect [1–5]. A bigger similarity expresses a greater matching quantity and more information, and a smaller similarity describes a lower matching quantity and lesser information. The two principal categories of image matching are grayscale-based and feature-based methodologies. By facilitating the similarity between the two photographs, the grayscale-based methodology aligns the template photograph with the original photograph's location and measures the precision and successful degree of matching. The essential elements of a photograph for matching in the feature-based methodology are margins, borders, texture, entropy, electricity, coloration, intersections, etc. The stability and quality of the chosen photograph attributes investigate the technology's cumulative efficiency. Template matching technology can efficiently and expeditiously recognize images, facilitating the wide-ranging utilization of target image recognition, such as medical diagnosis, pattern recognition, remote sensing mapping, military guidance, industrial component detection, environmental monitoring, etc.

The image acquisition is affected by the position, time, light, angle, object shape and multi-sensors, and the image obtained from the same scene may be distorted. Various matching technologies perform complicated operations for image matching to achieve image collection and information extraction, such as normalized cross-correlation, distance template, SIFT operator, and atomic potential field matching. These approaches have simplified estimation forms and desire minimal destination information, the security and precision of matching are guaranteed as the detected item does not obstruct it, particularly when non-contact measurement is appropriate. However, classical template matching has multiple drawbacks: susceptible to target geometric deformation and grayscale distortion, intuitive to remove degeneration after rotation, incurs substantial cumulative errors, significant information processing complexity, generates combinatorial explosion, precision and velocity that are insufficient for practical applications. Recently, numerous optimization approaches have been presented to address image matching, such as aquila optimization (AO) [6], dingo optimization algorithm (DOA) [7], spotted hyena optimizer (SHO) [8], slime mould algorithm (SMA) [9], seagull optimization algorithm (SOA) [10], sooty tern optimization algorithm (STOA) [11], tunicate swarm algorithm (TSA) [12].

Si et al. initiated an automatic pattern estimation genetic algorithm that utilized a mutation technique and self-awareness crossing supervisor to remedy image matching, this mentioned algorithm displayed substantial sustainability and durability to prohibit precocious convergence, accelerate integration frequency and attain greater matching proficiency [13]. Mousavi et al. constructed a dual-stage descriptor-based keypoint screening technique that utilized a mean-shift clustering procedure to assess the productivity and precision of image matching, a numerical index and confusion elimination were incorporated into the mentioned technique to arrive at and screen out the remaining disoriented key points [14]. Liu et al. recommended an altered firework method to remedy the color image attribute matching by altering the firework detonation distance and detonation quantity, this mentioned method maintained durable durability and dependability in retaining the color image's essential feature areas and extending noticeably greater color image matching precision and productivity [15]. Wang et al. created an innovative objective monitoring technique based on stackable polygonal matching and multiscale investigation, this mentioned technique exhibited reliable tracking precision and excessive matching productivity by measuring an appropriate radial distance and assessing the similarity [16]. Cui et al. employed a flexible juxtapose threshold scale-invariant feature conversion approach that utilized photograph complexity estimation to remedy the remotely sensed image matching,

this mentioned approach retrieved the advisable points to accomplish upgraded profound sustainability and near-real-time accuracy [17]. Liu et al. released a parallel technique that utilized hausdorff proximity to remedy the image matching, this mentioned technique featured extreme parallelism and scalability to regulate stochastic vibration, disregard photograph clamor collaboration, and deliver the strongest matching impact [18]. Tamilkodi et al. crafted a weighted cutting-edge matching retrieval technique to remedy image extraction, this mentioned technique employed an integration procedure of extracting color, texture, and shape attributes from the image, which displayed substantial reliability and durability to attain faster recall productivity and higher matching precision [19]. Srinivasa et al. advised a 3-D photograph skeletonization approach to remedy the shape matching, this mentioned approach delivered field-programmable arrays to alleviate resource requirements and attain greater matching precision [20]. Lu et al. initiated an altered graph cut stereo matching methodology established on survey transformation to remedy the stereo matching, the hamming separation of the appropriate pixel is constructed as the similarity, this mentioned methodology exhibited adequate stability and durability to attain a greater stereo matching precision [21]. Nie et al. advised an alternative approach that integrated the ant colony optimization with 3D particle matching technique, this mentioned approach exhibited durable stability and reliability to refresh the particle monitoring velocimetry, minimize the displacement-pattern value and acquire the augmented matching precision and resolution efficiency [22]. Wang et al. pursued a profitable image matching approach to correlate conspicuous features in visual remote-sensing photographs, this mentioned approach seamlessly integrated line segment definition and characteristic matching to maximize matching quality and convergence impact [23]. Shao et al. identified a trustworthy and durable feature point matching system that utilized minimum motion-related entropy to upgrade feature-matching precision, this mentioned system maintained remarkable robustness and magnificent feature-matching profitability [24]. Xiang et al. originated a golden sine cosine salp swarm technique with an unpredictable neighbor discovery strategy to remedy the shape matching, this mentioned technique displayed certain superiority and dependability to maintain discovery and extraction and establish the greatest matching quality [25]. Rosenke et al. invented a generic mixed technique centered on discretization structure to remedy the image matching, this mentioned technique possessed excellent consistency and reliability for accomplishing affine modifications and multiple combinations of scaling, rotation, and translation [26]. Liu et al. explored hypothetical verification to construct an e-commerce customer categorization system that utilized an augmented 3-D block matching technique and conducted a performance evaluation, this mentioned system exhibited excellent robustness and dependability to gather the greatest solution [27]. Shao et al. discovered an innovative navigational visual method to remedy the lander's attitude and location, this mentioned method accomplished accurate pin-point descending and eliminated the cumulative error of juxtaposed navigation to attain high matching precision and substantial stability [28]. Shen et al. identified a subdivision selection methodology to remedy rapid and precise video event identification and productivity of the mentioned methodology integrating projections in identifying individuals activities have been confirmed [29]. Liu et al. advised a productive metrics training methodology to cultivate competitive instances that are authorized to deliver durable separation metrics, this mentioned methodology exhibited courageous consistency and dependability to safeguard the re-ID models against feature disruption assaults and yield accurate predictions [30]. To summarize, These algorithms can successfully maintain an equilibrium between discovery and extraction to refrain from preterm convergence and anticipation stagnation and exhibit fantastic durability and adaptability to furnish superior matching effectiveness and precision.

The GJO is motivated by the jackal's synchronized foraging that emphasizes the strategy of scavenging for prey, wrapping around prey and attacking prey to deliver the most outstanding value, which has substantial sustainability and durability to prohibit precocious convergence, accelerate convergence frequency and attain greater matching proficiency [31]. The lateral inhibition inhibits visual information loss, strengthens the gray gradient and spatial resolution, upgrades the photograph matching precision, promotes image contrast, and amplifies the visible foreground and background [32]. The LI-GJO integrates the natural combination and complementary benefits to eliminate exploration stagnation and recognize the most suitable solution. The LI-GJO is utilized to accomplish image matching, and the stated intention is to execute a pixel-for-pixel comparison methodology to locate the appropriate portion of the template photograph in the original photograph and guarantee the matching precision by assessing the similarities or distinctions between the two photographs. The experimental conclusions exhibit that the LI-GJO equalizes discovery and extraction to prohibit precocious convergence, which has substantial durability and dependability to acquire a higher anticipated precision, a greater matching proficiency, better convergence effectiveness and stronger stability.

The article is scheduled as follows: Section 2 manifests GJO. Section 3 explores lateral inhibition. Section 4 generates the hybrid GJO and lateral inhibition. Section 5 extends the experimental comparison and outcome. Section 6 portrays the conclusion and future research.

2 GJO

The GJO utilizes the cooperative hunting measures of jackal pairs to capture the best prey, which includes three crucial search processes: scavenging for prey, wrapping around prey and attacking prey, which is exhibited in Fig. 1. The GJO manipulates discovery and extraction to arrive at exceptional measured precision and prompt convergence productivity.

Fig. 1 **A** A jackal pair (**B**) scavenging for prey (**C**) Tracking and wrapping around prey (**D** & **E**) attacking prey

2.1 Search domain model

The initialization of the jackal is constructed as:

$$Y_0 = Y_{\min} + rand\left(Y_{\max} - Y_{\min}\right) \tag{1}$$

where $Y_{\max}$ and $Y_{\min}$ embody the control interval, $Y_{\max}$ embodies the initial position, *rand* embodies a variable in [0,1].

In GJO, two fittest individuals embody a jackal pair, which is constructed as:

$$Prey = \begin{bmatrix} Y_{1,1} & Y_{1,2} & \cdots & Y_{1,d} \\ Y_{2,1} & Y_{2,2} & \cdots & Y_{2,d} \\ \vdots & \vdots & \vdots & \vdots \\ Y_{n,1} & Y_{n,2} & \cdots & Y_{n,d} \end{bmatrix} \tag{2}$$

where $Y_{i,j}$ embodies the *jth* position of *ith* prey, n embodies the total prey, d embodies the issue dimension. The F_{OA} is constructed as:

$$F_{OA} = \begin{bmatrix} f(Y_{1,1};Y_{1,2};Y_{1,d}) \\ f(Y_{2,1};Y_{2,2};Y_{2,d}) \\ \vdots \\ f(Y_{n,1};Y_{n,2};Y_{n,d}) \end{bmatrix} \tag{3}$$

where f embodies the objective function, F_{OA} embodies the fitness value matrix.

2.2 Exploration

The jackal utilizes its distinctive predation structure to perceive the surrounding area and investigate prey. Once the jackal finds the prey, the pair based on mutual collaborative hunting behavior will quickly surround and capture the prey. The positions are constructed as:

$$Y_1(t) = Y_M(t) - E \cdot \left|Y_M(t) - rl \cdot Prey(t)\right| \tag{4}$$

$$Y_2(t) = Y_{FM}(t) - E \cdot \left|Y_{FM}(t) - rl \cdot Prey(t)\right| \tag{5}$$

where t embodies the nowaday iteration, $Prey(t)$ embodies the nowaday prey, $Y_M(t)$ and $Y_{FM}(t)$ embody the jackal pair's nowaday positions, $Y_1(t)$ and $Y_2(t)$ embody the refreshed jackal pair's positions.

The evading energy E is constructed as:

$$E = E_1 * E_0 \tag{6}$$

where E_1 embodies a reduction process of prey energy, E_0 embodies an initial value of prey energy.

$$E_0 = 2 * r - 1 \tag{7}$$

where r embodies a variable in [0,1].

$$E_1 = c_1 * (1 - (t/T)) \tag{8}$$

where T embodies the maximum iteration, c_1 embodies a constant 1.5, and E_1 decays linearly.

The rl is constructed as:

$$rl = 0.05 * LF(y) \tag{9}$$

The LF is the target fitness of the Lévy, which is constructed as:

$$LF(y) = 0.01 \times (\mu \times \sigma)/\left(\left|v^{(1/\beta)}\right|\right); \sigma = \left(\frac{r(1+\beta) \times sin(\pi\beta/2)}{r\left(\frac{1+\beta}{2}\right) \times \beta \times \left(2^{\frac{\beta-1}{2}}\right)}\right)^{1/\beta} \tag{10}$$

where μ and v embody the variables in (0,1), β embodies 1.5.

The refreshed jackal's position is constructed as:

$$Y(t+1) = \frac{Y_1(t) + Y_2(t)}{2} \tag{11}$$

2.3 Exploitation

The evading energy will decrease rapidly once the prey is found and threatened. The golden jackal will encircle, attack and consume prey. The jackal pair's capture technique is constructed as:

$$Y_1(t) = Y_M(t) - E \cdot \left|rl \cdot Y_M(t) - Prey(t)\right| \tag{12}$$

$$Y_2(t) = Y_{FM}(t) - E \cdot \left|rl \cdot Y_{FM}(t) - Prey(t)\right| \tag{13}$$

where t embodies the nowaday iteration, $Prey(t)$ embodies the nowaday prey, $Y_M(t)$ and $Y_{FM}(t)$ embody a jackal pair's nowaday positions, $Y_1(t)$ and $Y_2(t)$ embody a jackal pair's refreshed positions. Formula (11) yields the refreshed jackal's position.

To illustrate the solution phase further, the pseudocode of GJO is displayed in Algorithm 1.

Algorithm 1 GJO

Step 1. Initialize the arbitrary prey size $Y_i(i = 1, 2, ..., n)$

Step 2. Assess prey's fitness

Retrieve male jackal Y_1, female jackal Y_2

Step 3. while ($t < T$) do

for each prey

Revisit the evading energy E via Eqs. (6), (7) and (8)

Revisit rl via Eqs. (9) and (10)

if ($|E| \geq 1$)

Revisit the prey position via Eqs. (4), (5) and (11)

else ($|E| < 1$)

Revisit the prey position via Eqs. (12), (13) and (11)

end if

end for

Validate if any prey spans the detection area and customize it

Assess the fitness of each prey

Revisit Y_1 if there is a superior prey

$t = t + 1$

end while

Return Y_1

3 Lateral inhibition

The lateral inhibition has been found and confirmed by Hartline in the electrophysiological experiment on tachypleus vision. Each eyelet of tachypleus compound eye is equivalent to a receptor, which is a neural network composed of a unique optical system, sensory cells and nerve fibers. Each optical system of tachypleus has an associated inhibitory field around it. When the receptors are exposed to different light intensities, the electric pulse intensity and nerve excitation have some changes, and it is extremely easy to generate maximum or minimum values.

The lateral inhibition mechanism can avoid visual information loss, improve image contrast, enhance the gray gradient, and strengthen the visual foreground and background. The lateral inhibition preprocessess the original and template images, which considerably enhances the precision, dependability and spatial resolution of template matching, that is constructed as:

$$r_p = e_p + \sum_{j=1}^{n} k_{p,j}\left(r_j - r_{p,j}\right), p = 1, 2, ..., n; j \neq p \tag{14}$$

where e_p and r_p embody the input and output of *pth* receptor, $k_{p,j}$ embodies a coefficient.

To calculate efficiently, the lateral inhibition is modified to a 2D gray. The gray intensity of image pixel (m, n) is constructed as:

$$R(m,n) = I_0(m,n) + \sum_{i=-M}^{M} \sum_{j=-N}^{N} \alpha_{i,j} I_0(m+i, n+j) \tag{15}$$

where $\alpha_{i,j}$ embodies a coefficient between point (i, j) and centroid point, $I_0(m, n)$ embodies the initial gray intensity of point (m, n), $R(m, n)$ embodies the gray intensity of point (m, n) after preprocessing via lateral inhibition, $M \times N$ embodies the area of the acceptable domain. The schematic representation when $M = N = 2$ is exhibited in Fig. 2.

The corresponding distance has an inverse relationship with the competition coefficient. The strength of the inhibitory impact increases with decreasing distance from the receptor. The range of the receptor is 5×5, which is constructed as:

$$R(m,n) = I_0(m,n) + \sum_{i=-M}^{M} \sum_{j=-N}^{N} \alpha_{i,j} I_0(m+i, n+j) \tag{16}$$

Since visual neurons are all at the same input level, the competing coefficient is infinitely close to zero, which is constructed as:

$$\alpha_0 + 8\alpha_1 + 16\alpha_2 = 0 \tag{17}$$

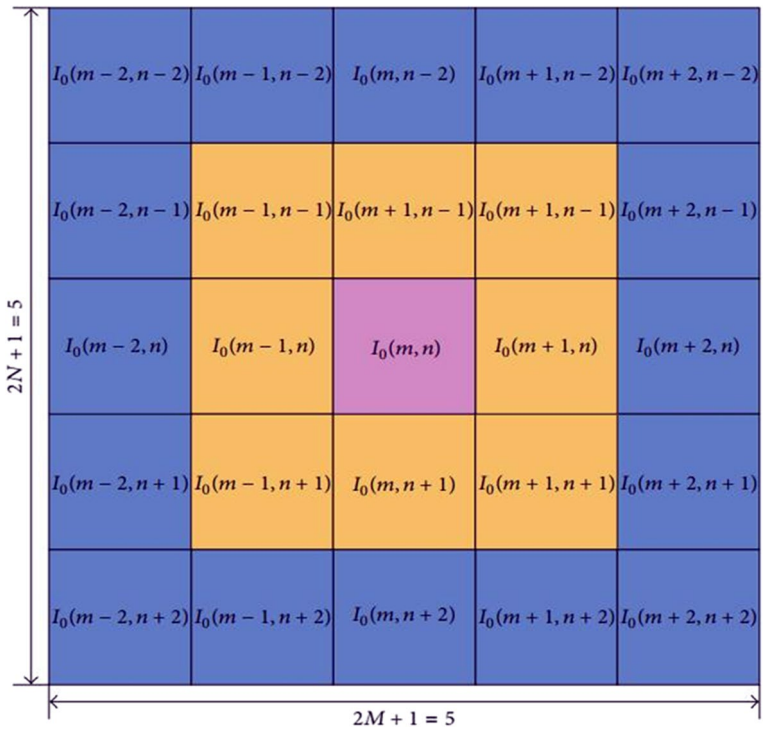

Fig. 2 Schematic representation via lateral inhibition structure when $M = N = 2$

where α_0=1, $\alpha_1 = -0.075$, and $\alpha_2 = -0.025$. The matrix model is constructed as:

$$U = \begin{bmatrix} -0.025 & -0.025 & -0.025 & -0.025 & -0.025 \\ -0.025 & -0.075 & -0.075 & -0.075 & -0.025 \\ -0.025 & -0.075 & 1 & -0.075 & -0.025 \\ -0.025 & -0.075 & -0.075 & -0.075 & -0.025 \\ -0.025 & -0.025 & -0.025 & -0.025 & -0.025 \end{bmatrix} \tag{18}$$

The template U is coupled with $R(m, n)$ to create a fresh gray intensity and retrieve the edge information.

$$F(m,n) = \begin{cases} 0 & R(m,n) \leq T \\ 255 & R(m,n) > T \end{cases} \tag{19}$$

where T embodies the threshold set by actual condition, and $F(m, n)$ embodies a gray intensity of point (m, n) after multiple operations.

4 LI-GJO

4.1 The fitness of LI-GJO

The fitness is utilized to measure the jackal's fitness in accordance with actual situation and particular operation. If the matched image has a noteworthy size, the LI-GJO will consume longer to estimate the fitness. The schematic representation of the template operation is exhibited in Fig. 3.

The objective function is constructed as:

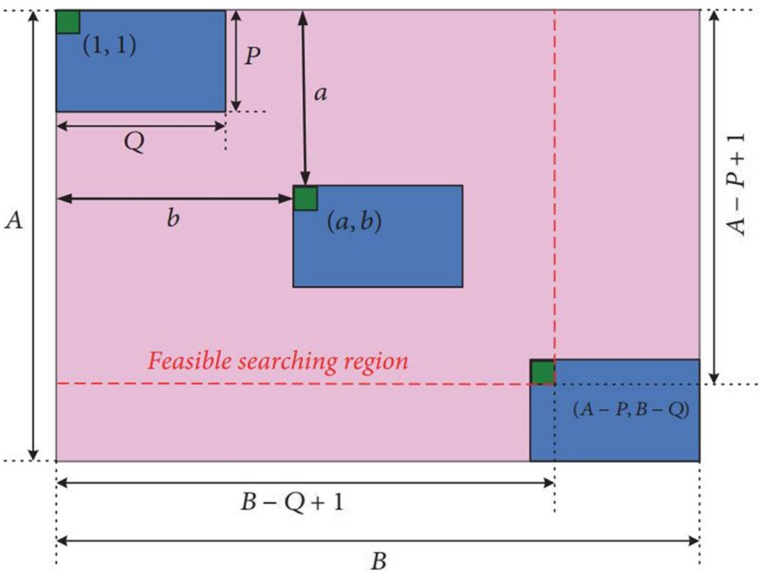

Fig. 3 Schematic representation of the template operation

$$f(m,n) = \frac{1}{PQ} \sum_{i=0}^{P-1} \sum_{j=0}^{Q-1} I(m+i, n+j) \tag{20}$$

where $P \times Q$ embodies the size of template photograph (m,n); $I(m+i, n+j)$ embodies the preprocessed gray intensity of the $(m+i, n+j)$. If the original photograph's size is $A \times B$, a coordinate interval of original photograph for template matching is $1 \le m \le A - P + 1$ and $1 \le n \le B - Q + 1$.

4.2 The procedure of LI-GJO

The pseudocode of the LI-GJO is displayed in Algorithm 2. The flow chart of the LI-GJO for image matching is exhibited in Fig. 4.

Algorithm 2 LI-GJO

Step 1. Image preparation. Grayscale photographs are constructed by converting both original photograph and template photograph, execute a filter to mitigate the noise, integrate the lateral inhibition to preprocess the photograph via Eqs. (16) - (19), which is conducive to background suppression and target enhancement, thereby reducing image noise and improving the signal-to-noise ratio

Step 2. Initialize the arbitrary LI-GJO prey size $Y_i(i = 1, 2, ..., n)$; control parameters E, rl; problem dimension D; the maximum iteration T. $D = 2$ is the image dimension

Step 3. Assess the respective fitness of each prey

Step 4. Explore the finest prey in the search scope

Step 5. Revisit E, rl

Step 6. Revisit the position of the nowaday prey via Eqs. (1)-(13)

Step 7. If $t < T$ is not satisfied, return to step 3

Step 8. Return Y_1

5 Experimental comparison and outcome

5.1 Experimental configuration

The experimental configuration is maintained on a computer with an Intel Core i9-12900HX 2.30 GHz CPU, RTX 3080 Ti, and 64 GB RAM. Each technique is scheduled in MATLAB R2018b.

5.2 Configuring parameters

To guarantee the profitability and practicability, LI-GJO is contrasted with LI-AO, LI-DOA, LI-SHO, LI-SMA, LI-SOA, LI-STOA and LI-TSA. Configuring parameters of each

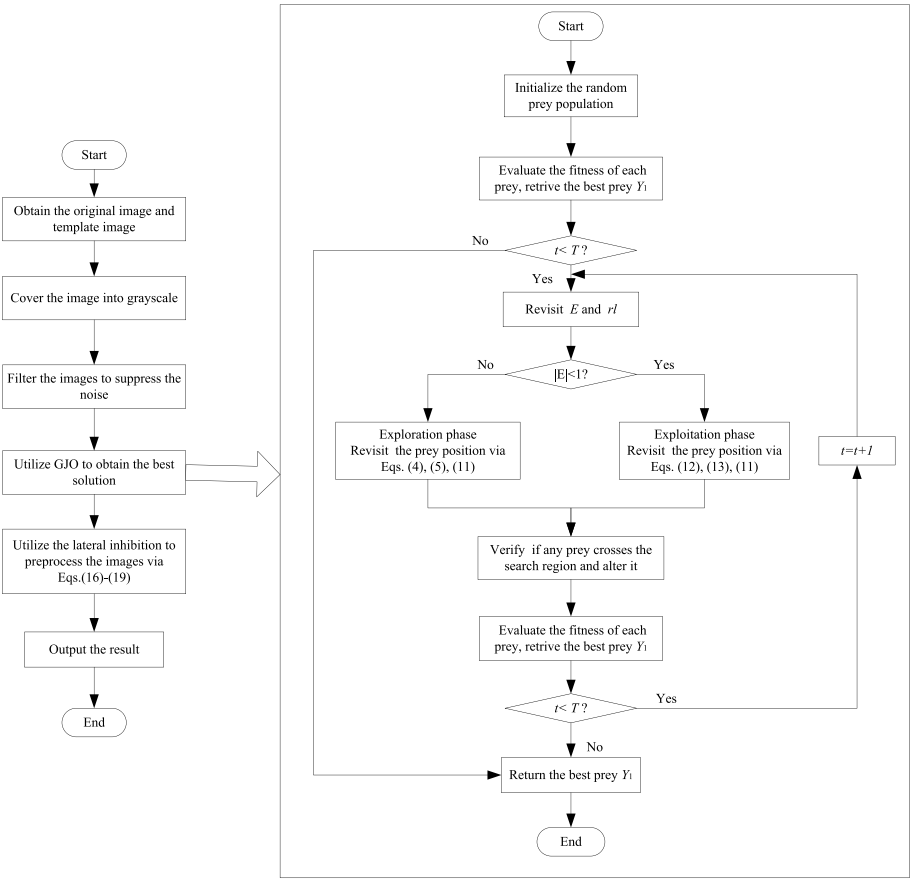

Fig. 4 Flow chart of the LI-GJO for image matching

technique are trustworthy and representative values of the original research, which are depicted in Table 1.

5.3 The outcomes and analysis

For various techniques, the population amount is 100, the greatest iteration is 300, and the standalone procedure is 30. Best, Worst, Mean and Std are the optimal solution, worst solution, mean solution and standard deviation. CR is the correct rate, time is the execution time, and standard deviation is employed to establish the ranking. These important indicators are used to detect the success rate and matching accuracy of the template image. The LI-GJO is contrasted with other algorithms to confirm the matching performance and optimization efficiency, the threshold value of extracted edge image is defined $T = 110$. The comparative results accomplished utilizing various algorithms are depicted in Table 2.

The GJO utilizes a cooperative predation mechanism to search, enclose and capture the prey. The GJO not only has strong stability and robustness to promote the

Table 1 Configuring parameters of each technique

Technique	Parameter	Value
LI-AO	Irregular number *rand*	[0,1]
	Unaltered value s	0.01
	Irregular number u	[0,1]
	Irregular number v	[0,1]
	Unaltered value β	1.5
	Unaltered value U	0.00565
	Unaltered value ω	0.005
	Irregular number α	(0,1)
	Irregular number δ	(0,1)
LI-DOA	Irregular vector a_1	[0,1]
	Irregular vector a_2	[0,1]
	Irregular vector A	(1,0)
	Irregular vector B	(1,1)
	Irregular number b	(0,3)
LI-SHO	Irregular number r_1	[0,1]
	Irregular number r_2	[0,1]
	Irregular vector M	[0.5,1]
	Irregular vector h	[0,5]
LI-SMA	Irregular vector r	[0,1]
	Irregular vector *rand*	[0,1]
LI-SOA	Unaltered value f_c	2
	Unaltered value u	1
	Unaltered value v	1
	Irregular number *rd*	[0,1]
	Irregular number k	$[0, 2\pi]$
LI-STOA	Unaltered value C_f	2
	Irregular number R_{rand}	[0,1]
	Irregular number i	$[0, 2\pi]$
	Unaltered value u	1
	Unaltered value v	1
LI-TSA	Irregular number C_1	[0,1]
	Irregular number C_2	[0,1]
	Irregular number C_3	[0,1]
	Unaltered value $P_{\min}$	1
	Unaltered value $P_{\max}$	4
	Irregular number r_{and}	[0,1]
LI-GJO	Irregular number *rand*	[0,1]
	Irregular number r	[0,1]
	Unaltered value c_1	1.5
	Irregular number u	(0,1)
	Irregular number v	(0,1)
	Unaltered value β	1.5

Table 2 Comparative results accomplished utilizing various algorithms

Image	Result	LI-AO	LI-DOA	LI-SHO	LI-SMA	LI-SOA	LI-STOA	LI-TSA	LI-GJO
Test 1	Best	3262	3262	3262	3262	3262	3262	3262	3262
	Worst	3240	3042	2936	2833	3204	3185	2298	3262
	Mean	3257.6	3245.1	3101.7	3233.4	3254.5	3249	3133.5	3262
	Std	8.9504	48.7716	82.5747	108.8408	16.0231	24.4293	333.2991	0
	CR	80.00%	83.33%	3.33%	93.33%	76.67%	70.00%	86.67%	100%
	Time	16.8481	13.5263	14.0485	12.2764	11.8714	11.8004	11.3939	11.2851
	Rank	2	5	6	7	3	4	8	1
Test 2	Best	39399	39399	39399	39399	39399	39399	39399	39399
	Worst	36964	35446	34074	39399	36555	36555	32054	39399
	Mean	39237	38237	35646	39399	37927	38142	38175	39399
	Std	617.7793	1476.7	958.4521	0	1227.2	1285.8	2784.1	0
	CR	93.33%	60.00%	3.33%	100%	40.00%	50.00%	83.33%	100%
	Time	154.1916	101.3517	106.0142	97.5667	101.4715	102.9230	91.8519	90.4561
	Rank	2	6	3	1	4	5	7	1
Test 3	Best	3678	3678	3678	3678	3678	3678	3678	3678
	Worst	3678	3644	3572	3167	3648	3648	3090	3678
	Mean	3678	3669.1	3632.4	3643.9	3669.4	3670.4	3393.7	3678
	Std	0	12.9794	30.5125	129.6449	12.4751	11.8891	255.2680	0
	CR	100%	66.67%	16.67%	93.33%	66.67%	70.00%	43.33%	100%
	Time	17.6609	11.8944	10.5522	10.9368	9.9577	9.7247	10.0022	9.3462
	Rank	1	4	5	6	3	2	7	1
Test 4	Best	1619	1619	1607	1619	1619	1619	1619	1619
	Worst	1568	1566	1535	1505	1602	1607	1462	1619
	Mean	1613.9	1604.9	1582.8	1613.8	1617.4	1618.2	1569.4	1619
	Std	12.2889	16.9704	18.1534	21.9901	4.9930	3.0445	57.1155	0
	CR	76.67%	46.67%	0%	93.33%	90.00%	93.33%	53.33%	100%
	Time	9.7337	8.2331	7.1652	8.0478	6.0874	6.0240	5.7308	5.4148
	Rank	4	5	6	7	3	2	8	1
Test 5	Best	14741	14741	14741	14741	14741	14741	14741	14741
	Worst	14704	14688	14655	14741	14712	14712	13030	14741
	Mean	14732	14728	14702	14741	14734	14736	14114	14741
	Std	15.9865	19.4066	22.6979	0	7.3423	7.37	838.6167	0
	CR	73.33%	63.33%	6.67%	100%	50.00%	60.00%	63.33%	100%
	Time	66.0185	43.4123	44.3410	40.2352	40.9742	41.1368	40.0014	39.9736
	Rank	4	5	6	1	2	3	7	1
Test 6	Best	3249	3249	3249	3249	3249	3249	3249	3249
	Worst	3211	3229	3184	3000	3238	3238	2833	3249
	Mean	3243.3	3246.4	3215.3	3209.2	3246.7	3246.2	3135.6	3249
	Std	12.9064	5.3478	20.0295	82.4911	2.9470	3.1914	141.8954	0
	CR	80.00%	70.00%	3.33%	80.00%	36.67%	43.33%	53.33%	100%
	Time	31.9584	22.6195	20.2567	19.4968	19.1011	19.1166	18.7242	18.5905
	Rank	5	4	6	7	2	3	8	1
Test 7	Best	7387	7387	7387	7387	7387	7387	7387	7387
	Worst	7268	7147	7193	6987	7250	7271	6567	7385

Table 2 (continued)

Image	Result	LI-AO	LI-DOA	LI-SHO	LI-SMA	LI-SOA	LI-STOA	LI-TSA	LI-GJO
	Mean	7361.8	7330.4	7281.9	7338.8	7351.7	7357.8	7199.8	7386.9
	Std	43.5946	61.0769	57.2892	80.8733	43.3016	36.7418	299.3029	0.5074
	CR	66.67%	43.33%	10.00%	60.00%	43.33%	33.33%	56.67%	93.33%
	Time	46.9655	30.3189	28.7788	24.4829	27.8762	27.9370	24.8872	23.9449
	Rank	4	6	5	7	3	2	8	1
Test 8	Best	4735	4735	4725	4735	4735	4735	4735	4735
	Worst	4725	4527	4530	4458	4710	4718	3986	4735
	Mean	4734	4720.4	4657.1	4716.5	4728.6	4730.1	4486.6	4735
	Std	3.0513	41.4342	45.6964	70.2772	7.5366	6.3122	312.0950	0
	CR	90.00%	76.67%	0%	93.33%	53.33%	60.00%	56.67%	100%
	Time	27.4103	18.6774	17.1113	15.4535	16.1512	16.0772	15.3534	14.8910
	Rank	2	5	6	7	4	3	8	1
Test 9	Best	3977	3977	3977	3977	3977	3977	3977	3977
	Worst	3973	3943	3662	3783	3965	3965	3382	3977
	Mean	3975.3	3970.4	3890.6	3941	3975.7	3975.3	3835.7	3977
	Std	2.0160	8.4877	119.5	73.5782	3.2092	3.2688	152.3599	0
	CR	56.67%	53.33%	6.67%	80.00%	80.00%	70.00%	46.67%	100%
	Time	19.5573	13.9895	12.8695	12.1060	11.9345	11.8273	11.1400	10.8526
	Rank	2	5	6	7	3	4	8	1
Test 10	Best	6078	6078	6078	6078	6078	6078	6078	6078
	Worst	4288	4281	4292	4267	4295	4298	4218	4358
	Mean	5374.3	5268.6	4713.6	4551.8	5477.5	5480.1	4823.4	5836.6
	Std	876.6623	761.6454	548.1475	609.1797	715.8418	703.3911	787.9902	559.2929
	CR	60.00%	30.00%	6.67%	13.33%	33.33%	40.00%	20.00%	83.33%
	Time	31.3365	23.1130	20.9131	19.6314	19.9509	19.6600	19.3138	18.6086
	Rank	8	6	1	3	5	4	7	2

computational efficiency but also uses exploration or exploitation to intensify the matching accuracy. The lateral inhibition effectively preprocesses the original image to eliminate the noise, avoid visual information loss, enhance the gray gradient, strengthen the visual foreground and background, accentuate the image features and maximize the matching effect. The LI-GJO intensifies the computational precision by combining the potential characteristics of the GJO and lateral inhibition. The LI-GJO has a large search domain to avert rapid convergence to locate the best solution. The stated intention is to execute a pixel-for-pixel comparison methodology to locate the appropriate portion of the template photograph in the original photograph and guarantee the matching precision by assessing the similarities or distinctions between the two photographs. The optimal solution and worst value embody discovery and extraction. The mean solution embodies the overall optimization level and convergence accuracy. The standard deviation embodies the stability. CR embodies the matching accuracy. The time reveals the matching efficiency. Through different evaluation indicators, the LI-GJO is contrasted to existing algorithms in toder to demonstrate the reliability and stability. For images 1, 2, 3, 4, 5, 6, 8 and 9, the optimal solution, worst solution and mean solution of LI-GJO are consistent and optimal, which implies that the LI-GJO has greater superiority and overall search

Table 3 Outcomes of *p-value* for Wilcoxon rank-sum

LI-GJO vs	LI-AO	LI-DOA	LI-SHO	LI-SMA	LI-SOA	LI-STOA	LI-TSA
Test 1	1.09E-02	2.16E-02	4.51E-12	1.61E-01	5.54E-03	1.36E-03	4.18E-02
Test 2	1.61E-01	1.44E-04	4.57E-12	N/A	8.10E-07	1.23E-05	2.14E-02
Test 3	N/A	6.46E-04	6.02E-10	1.61E-01	6.45E-04	1.34E-03	2.02E-06
Test 4	5.54E-03	5.32E-06	1.17E-12	1.61E-01	8.15E-02	1.61E-01	2.92E-05
Test 5	2.77E-03	3.13E-04	1.61E-11	N/A	1.02E-05	1.35E-04	2.85E-04
Test 6	1.10E-02	1.37E-03	4.49E-12	1.10E-02	2.67E-07	2.12E-06	2.90E-05
Test 7	6.94E-03	1.56E-05	1.98E-10	1.20E-03	1.89E-05	1.24E-06	6.87E-04
Test 8	8.14E-02	5.58E-03	1.20E-12	1.61E-01	2.87E-05	1.42E-04	6.44E-05
Test 9	5.59E-05	2.85E-05	1.58E-11	1.10E-02	1.10E-02	1.34E-03	5.26E-06
Test 10	1.24E-02	1.39E-04	2.82E-08	2.47E-09	4.73E-04	1.98E-03	2.08E-07

performance to explore the finest matching effect. The LI-GJO exhibits a lesser standard deviation and superior ranking, which implies that the LI-GJO has high stability. The correct rate of the LI-GJO is 100%, which implies that the LI-GJO has substantial global and local optimization to deliver an accurate solution. The completion time of the LI-GJO is relatively small, which implies that the LI-GJO has excellent operational efficiency. For image 7, all algorithms generate the exact solutions, but all evaluation indicators of the LI-GJO are superior to those of the LI-AO, LI-DOA, LI-SHO, LI-SMA, LI-SOA, LI-STOA and LI-TSA. The LI-GJO has a higher CR and quicker completion time, which implies that the LI-GJO can reasonably use exploration or exploitation to promote matching accuracy. For image 10, each algorithm obtains the same optimal value. The standard deviation of LI-GJO is lesser than that of LI-SHO, but the worst solution, mean solution, CR and completion time of LI-GJO are more productive than those of other techniques, the LI-GJO has excellent stability and high convergence effect. To summarize, the LI-GJO has superior durability and sustainability to obtain better evaluation indicators, which is an practical and usefull method to resolve the image matching.

The *p-value* Wilcoxon rank-sum [33] is depicted in Table 3, which is designed to investigate if two groups of data differ substantially. $p < 0.05$ implies a noteworthy discrepancy. $p \geq 0.05$ implies no noteworthy discrepancy. N/A implies "not applicable". The experimental conclusions exhibite that there is a substantial discrepancy between LI-GJO and other techniques.

The stated intention of template matching is to accurately align the original photograph with the template photograph and guarantee fitness value by measuring the similarity between two photographs, which is the area of focus for pattern recognition, image processing, computer vision and feature extraction. The experimental outcomes with the original photographs are exhibited in Figs. 5a, 6a, 7a, 8a, 9a, 10a, 11a, 12a, 13a and 14a and the template photographs are exhibited in Figs. 5b, 6b, 7b, 8b, 9b, 10b, 11b, 12b, 13b and 14b. The original photographs and template photographs extracted via the lateral inhibition are exhibited in Figs. 5c, 6c, 7c, 8c, 9c, 10c, 11c, 12c, 13c and 14c and Figs. 5d, 6d, 7d, 8d, 9d, 10d, 11d, 12d, 13d and 14d. The lateral inhibition mechanism preprocesses the original or template photograph to avoid visual information distortion, improve the gray gradient and spatial resolution, and enhance the image edges and background intensity, which remarkably intensifies the matching accuracy and computational efficiency. The final template matching outcomes ascertained via the LI-GJO are exhibited in Figs. 5e, 6e, 7e, 8e, 9e, 10e, 11e, 12e, 13e and 14e. The GJO, motivated by the jackal's

(a)

(b)

(c)

(d)

(e)

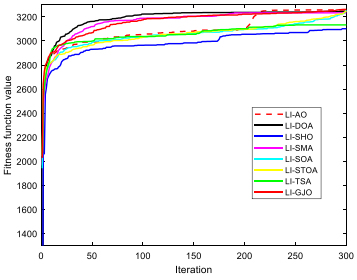

(f)

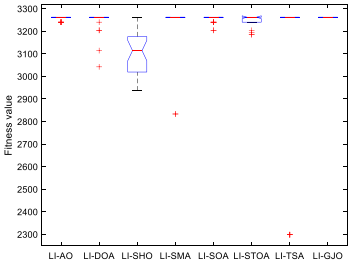

(g)

Fig. 5 Experimental outcomes for photograph 1. **a** Original photograph (1024×773). **b** Template photograph (68×61). **c** Original photograph extracted via the lateral inhibition. **d** Template photograph extracted via the lateral inhibition. **e** Ultimate template matching ascertained via LI-LWOA. **f** Convergence lines of experimental outcomes. **g** ANOVA of experimental outcomes

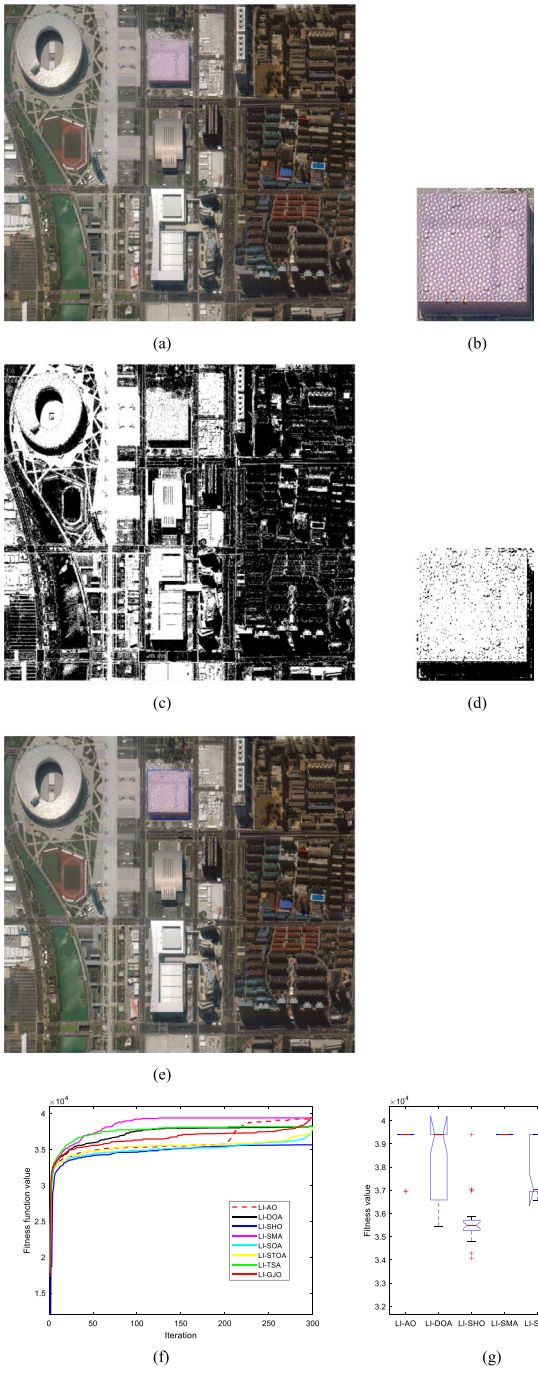

Fig. 6 Experimental outcomes for photograph 2. **a** Original photograph (1543 × 1393). **b** Template photograph (191 × 217). **c** Original photograph extracted via the lateral inhibition. **d** Template photograph extracted via the lateral inhibition. **e** Ultimate template matching ascertained via LI-LWOA. **f** Convergence lines of experimental outcomes. **g** ANOVA of experimental outcomes

(a)

(b)

(c)

(d)

(e)

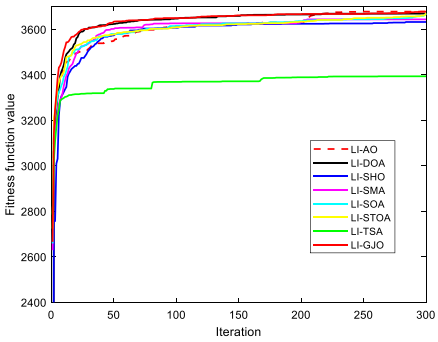

(f)

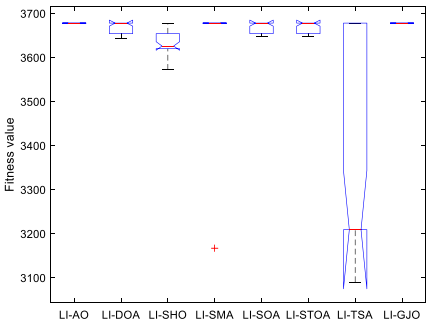

(g)

Fig. 7 Experimental outcomes for photograph 3. **a** Original photograph (670×325). **b** Template photograph (79×67). **c** Original photograph extracted via the lateral inhibition. **d** Template photograph extracted via the lateral inhibition. **e** Ultimate template matching ascertained via LI-LWOA. **f** Convergence lines of experimental outcomes. **g** ANOVA of experimental outcomes

(a)

(b)

(c)

(d)

(e)

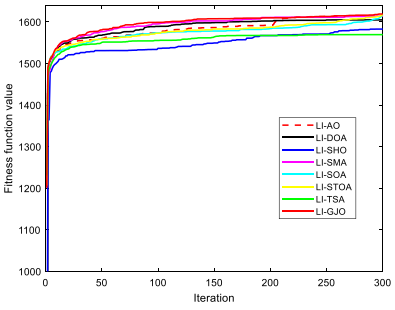

(f)

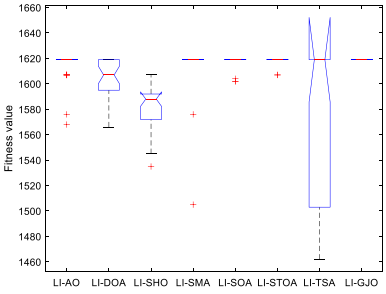

(g)

Fig. 8 Experimental outcomes for photograph 4. **a** Original photograph (800×533). **b** Template photograph (46×54). **c** Original photograph extracted via the lateral inhibition. **d** Template photograph extracted via the lateral inhibition. **e** Ultimate template matching ascertained via LI-LWOA. **f** Convergence lines of experimental outcomes. **g** ANOVA of experimental outcomes

(a)

(b)

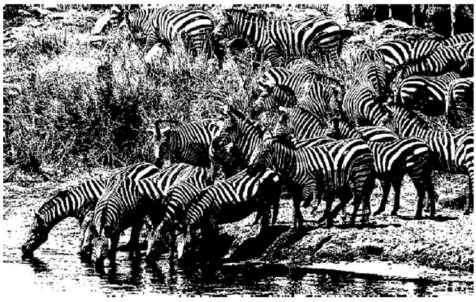

(c)

(d)

(e)

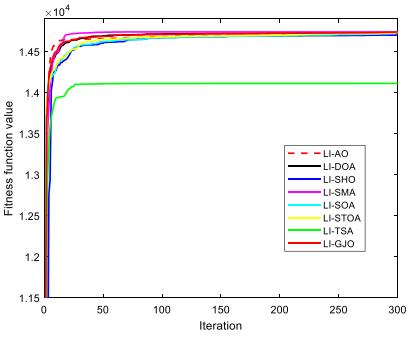

(f)

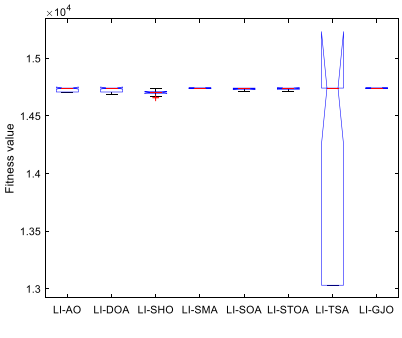

(g)

Fig. 9 Experimental outcomes for photograph 5. **a** Original photograph (900×562). **b** Template photograph (145×127). **c** Original photograph extracted via the lateral inhibition. **d** Template photograph extracted via the lateral inhibition. **e** Ultimate template matching ascertained via LI-LWOA. **f** Convergence lines of experimental outcomes. **g** ANOVA of experimental outcomes

(a)

(b)

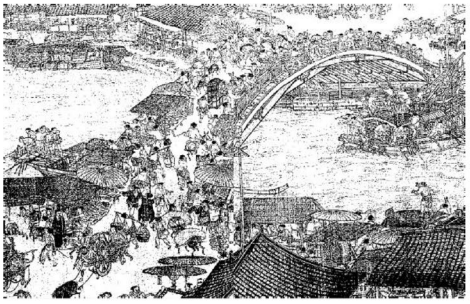

(c)

(d)

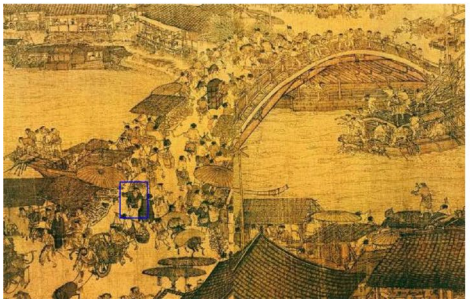

(e)

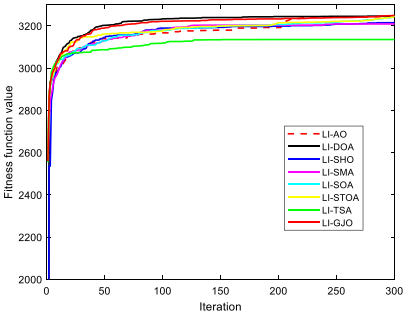

(f)

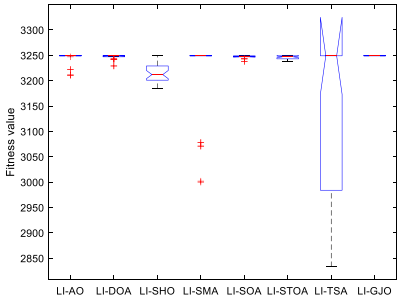

(g)

Fig. 10 Experimental outcomes for photograph 6. **a** Original photograph (1093 × 697). **b** Template photograph (67 × 87). **c** Original photograph extracted via the lateral inhibition. **d** Template photograph extracted via the lateral inhibition. **e** Ultimate template matching ascertained via LI-LWOA. **f** Convergence lines of experimental outcomes. **g** ANOVA of experimental outcomes

(a)

(b)

(c)

(d)

(e)

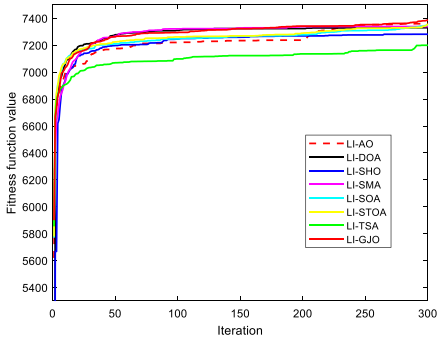

(f)

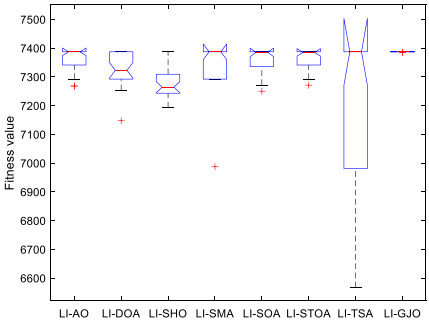

(g)

Fig. 11 Experimental outcomes for photograph 7. **a** Original photograph (1080×617). **b** Template photograph (73×153). **c** Original photograph extracted via the lateral inhibition. **d** Template photograph extracted via the lateral inhibition. **e** Ultimate template matching ascertained via LI-LWOA. **f** Convergence lines of experimental outcomes. **g** ANOVA of experimental outcomes

(a)

(b)

(c)

(d)

(e)

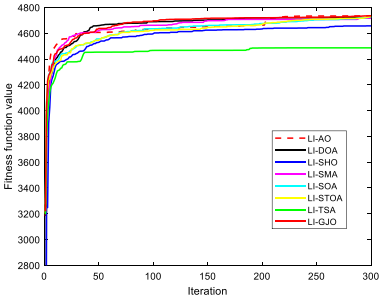

(f)

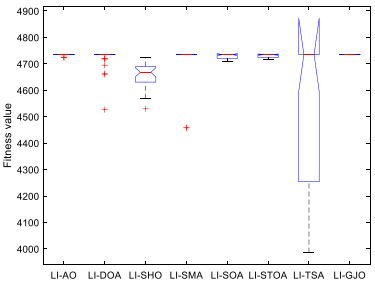

(g)

Fig. 12 Experimental outcomes for photograph 8. **a** Original photograph (1024×683). **b** Template photograph (98×71). **c** Original photograph extracted via the lateral inhibition. **d** Template photograph extracted via the lateral inhibition. **e** Ultimate template matching ascertained via LI-LWOA. **f** Convergence lines of experimental outcomes. **g** ANOVA of experimental outcomes

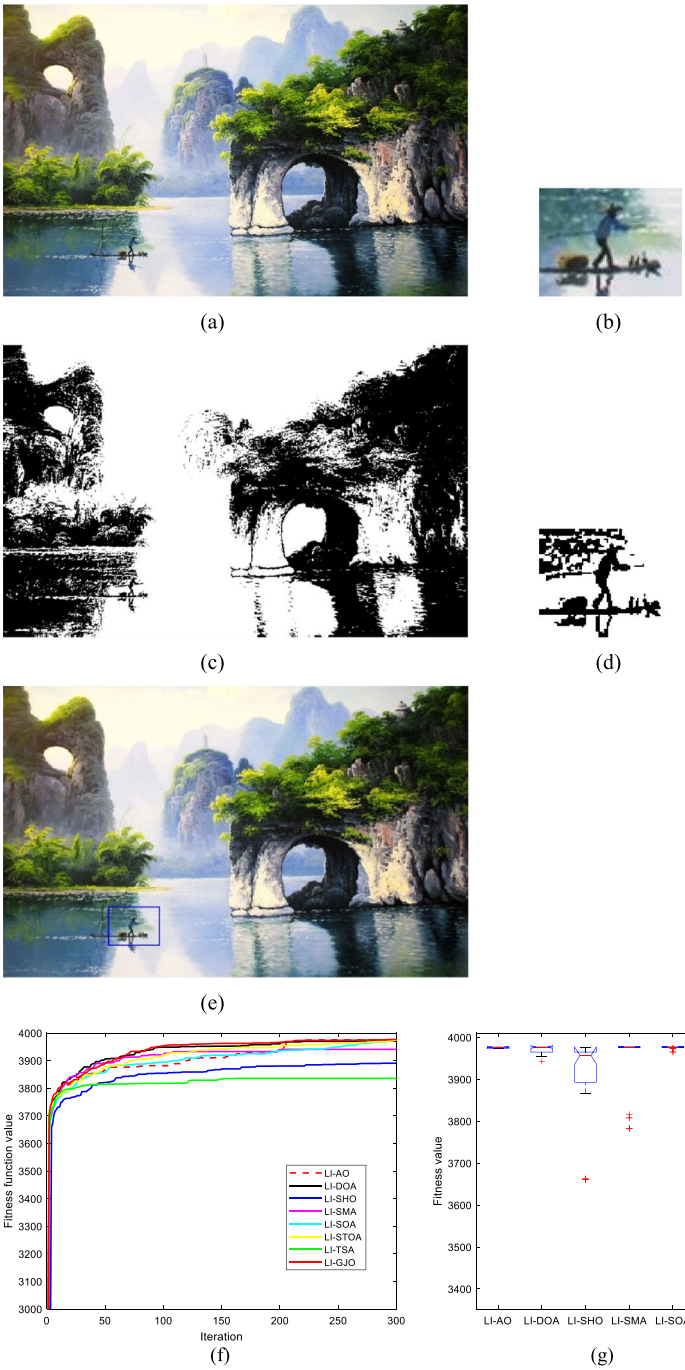

Fig. 13 Experimental outcomes for photograph 9. **a** Original photograph (780×490). **b** Template photograph (87×66). **c** Original photograph extracted via the lateral inhibition. **d** Template photograph extracted via the lateral inhibition. **e** Ultimate template matching ascertained via LI-LWOA. **f** Convergence lines of experimental outcomes. **g** ANOVA of experimental outcomes

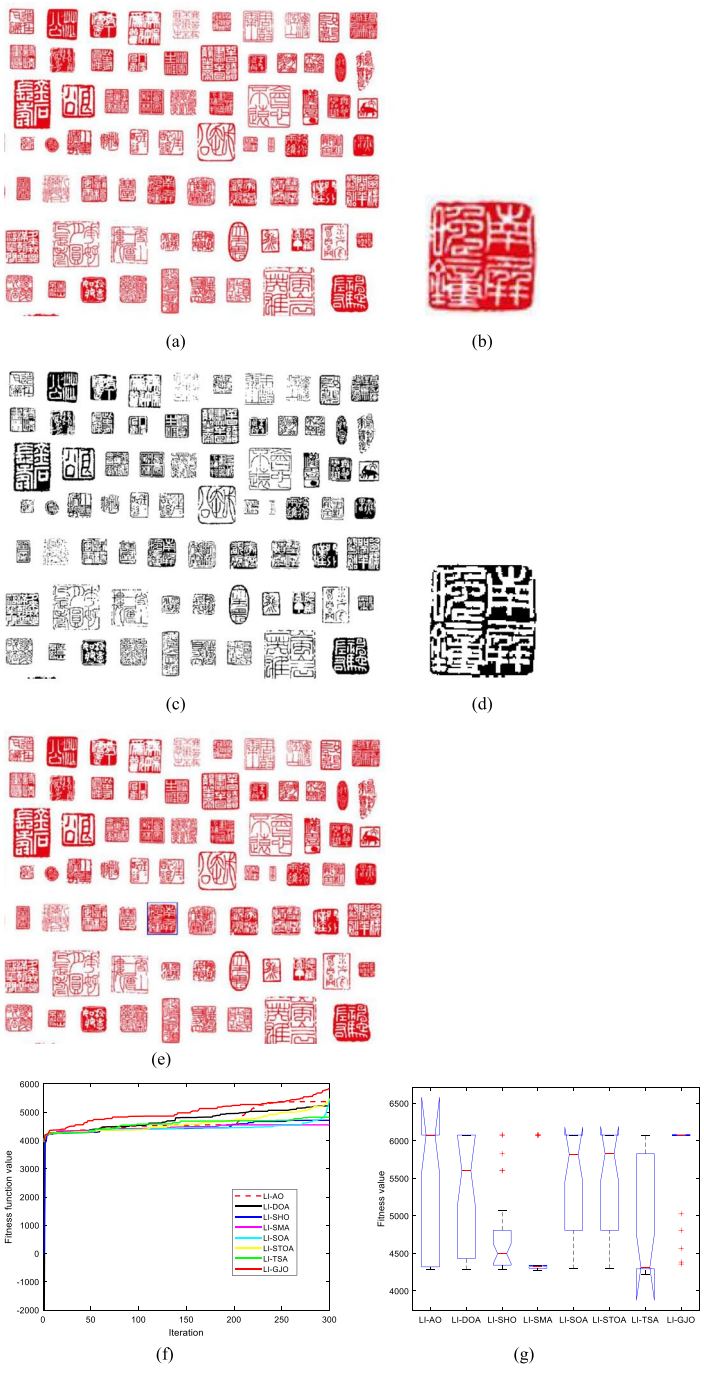

Fig. 14 Experimental outcomes for photograph 10. **a** Original photograph (1065 × 879). **b** Template photograph (85 × 90). **c** Original photograph extracted via the lateral inhibition. **d** Template photograph extracted via the lateral inhibition. **e** Ultimate template matching ascertained via LI-LWOA. **f** Convergence lines of experimental outcomes. **g** ANOVA of experimental outcomes

synchronized foraging, exhibits its procedure of scavenging for prey, wrapping around prey and attacking prey to furnish the most appropriate solution. The lateral inhibition improves the characteristics of the test image and enhances the stability of template matching, which contributes to boosting the calculation accuracy. The template photograph and the original photograph can be perfectly matched by the LI-GJO, which implies that the LI-GJO has excellent robustness and stability. Compared with LI-AO, LI-DOA, LI-SHO, LI-SMA, LI-SOA, LI-STOA and LI-TSA, the optimal solution, worst solution, mean solution, standard deviation, CR, completion time and ranking of the LI-GJO are superior, which implies that the LI-GJO utilizes the unique optimization mechanism to obtain higher calculational efficiency and greater matching accuracy. The convergence lines of experimental outcomes are exhibited in Figs. 5f, 6f, 7f, 8f, 9f, 10f, 11f, 12f, 13f and 14f. Compared with other techniques, the LI-GJO exhibits greater matching precision, superior measured accuracy and greater convergence frequency. The ANOVA tests of experimental outcomes are exhibited in Figs. 5g, 6g, 7g, 8g, 9g, 10g, 11g, 12g, 13g and 14g. The LI-GJO exhibits attractive sustainability and dependability to attain a lower standard deviation. To summarize, the LI-GJO delivers superiority and feasibility to resolve image matching.

6 Conclusion and future research

The GJO is motivated by the jackal's synchronized foraging that emphasizes the strategy of scavenging for prey, wrapping around prey and attacking prey to deliver the most outstanding value. The lateral inhibition inhibits visual information loss, strengthens the gray gradient and spatial resolution, upgrades the photograph matching precision, promotes image contrast, and amplifies the visible foreground and background. The LI-GJO employs natural combinations and complementary benefits to prohibit precocious convergence and deliver the most suitable value. The LI-GJO is integrated to address the image matching and confirm sustainability and durability. The stated intention is to execute a pixel-for-pixel comparison methodology to locate the appropriate portion of the template photograph in the original photograph and guarantee the matching precision by assessing the similarities or distinctions between the two photographs. The experimental outcomes are utilised to estimate each technique's aggregate matching impact and measured accuracy. The evaluation indicators of the LI-GJO are superior to those of LI-AO, LI-DOA, LI-SHO, LI-SMA, LI-SOA, LI-STOA and LI-TSA. The experimental outcomes imply that the LI-GJO can successfully balance exploration and exploitation to attain higher computational efficiency, better matching accuracy, and greater robustness and stability. Meanwhile, the LI-GJO has excellent practicality and stability and thus can efficaciously resolve the image matching.

In future work, the LI-GJO will be utilized to address complex image processing issues, such as sophisticated patterns, feature tracking, stereo matching and real-world images. Additionally, we will focus more on the theoretical study and mathematical model and investigate the astringency and implementation of the LI-GJO for image matching. The modified GJO will be utilized to address the shape matching via atomic potential function, further verifying the effectiveness and feasibility.

Acknowledgements This work was partially funded by Start-up Fund for Distinguished Scholars of West Anhui University under Grant Nos. WGKQ2022006, WGKQ2022050 and WGKQ2022052, the Scientific Research Projects of Universities in Anhui Province under Grant Nos. 2022AH051674 and 2022AH040241, the University Synergy Innovation Program of Anhui Province under Grant No. GXXT-2021-026, Smart Agriculture and Forestry and Smart Equipment Scientific Research and Innovation Team (Anhui Undergrowth Crop Intelligent Equipment Engineering Research Center) under Grant No. 2022AH010091, School-level quality engineering (school-enterprise cooperation development curriculum resource construction) under Grant No. wxxy2022101. The authors would like to thank the editor and anonymous reviewers for their helpful comments and suggestions.

Authors contribution **Jinzhong Zhang:** Conceptualization, Methodology, Software, Data curation, Formal analysis, Writing – original draft. **Gang Zhang:** Conceptualization, Methodology, Resources, Project administration, Funding acquisition. **Min Kong:** Conceptualization, Methodology, Writing – review & editing, investigation. **Tan Zhang:** Validation, Writing – review & editing. **Duansong Wang:** Project administration, Conceptualization, Supervision.

Data availability The data set (s) supporting the conclusions of this article is (are) included within the article.

Declarations

Competing interest The authors declare that they have no known competing financial interests or personal relationships that could have appeared to influence the work reported in this paper.

References

1. Ma X, Wang S, Liu W et al (2019) Optimized stereo matching algorithm for integral imaging microscopy and its potential use in precise 3-D optical manipulation. Opt Commun 430:374–379
2. Li M, Xie W (2019) Remote Sensing Image Matching Algorithm for Coastal Zone Based on Local Features. J Coast Res 93:723–728
3. Jaber MM, Ali MH, Abd SK et al (2022) A Machine Learning-Based Semantic Pattern Matching Model for Remote Sensing Data Registration. J Indian Soc Remote Sens 50:2303–2316
4. Chen S, Chen J, Rao Y et al (2022) A Hierarchical Consensus Attention Network for Feature Matching of Remote Sensing Images. IEEE Trans Geosci Remote Sens 60:1–11
5. Zhu S, Ma W, Yao J (2022) Global and local geometric constrained feature matching for high resolution remote sensing images. Comput Electr Eng 103:108337
6. Abualigah L, Yousri D, Abd Elaziz M et al (2021) Aquila optimizer: a novel meta-heuristic optimization algorithm. Comput Ind Eng 157:107250
7. Bairwa AK, Joshi S, Singh D (2021) Dingo optimizer: A nature-inspired metaheuristic approach for engineering problems. Math Probl Eng. https://doi.org/10.1155/2021/2571863
8. Dhiman G, Kumar V (2017) Spotted hyena optimizer: a novel bio-inspired based metaheuristic technique for engineering applications. Adv Eng Softw 114:48–70
9. Li S, Chen H, Wang M et al (2020) Slime mould algorithm: A new method for stochastic optimization. Future Gener Comput Syst 111:300–323
10. Dhiman G, Kumar V (2019) Seagull optimization algorithm: Theory and its applications for large-scale industrial engineering problems. Knowl-Based Syst 165:169–196
11. Dhiman G, Kaur A (2019) STOA: a bio-inspired based optimization algorithm for industrial engineering problems. Eng Appl Artif Intell 82:148–174
12. Kaur S, Awasthi LK, Sangal A, Dhiman G (2020) Tunicate Swarm Algorithm: A new bio-inspired based metaheuristic paradigm for global optimization. Eng Appl Artif Intell 90:103541
13. Si L, Hu X, Liu B (2022) Image Matching Algorithm Based on the Pattern Recognition Genetic Algorithm. Comput Intell Neurosci. https://doi.org/10.1155/2022/7760437
14. Mousavi V, Varshosaz M, Remondino F et al (2022) A Two-Step Descriptor-Based Keypoint Filtering Algorithm for Robust Image Matching. IEEE Trans Geosci Remote Sens 60:1–21
15. Liu D, Zhu H, Wang H (2022) Color Image Feature Matching Method Based on the Improved Firework Algorithm. Math Probl Eng. https://doi.org/10.1155/2022/9447410
16. Wang Y, Guo R, Zhao S (2022) Target tracking algorithm based on multiscale analysis and combinatorial matching. J Supercomput 78:12648–12661
17. Cui R, Wen M, Zhang K, Sun C (2021) Contrast threshold adaptive adjustment algorithm for remote sensing image matching. J Appl Remote Sens 15:036519
18. Liu Q, Peng H, Chen J, Gao H (2021) Design and implementation of parallel algorithm for image matching based on Hausdorff Distance. Microprocess Microsyst 82:103919
19. Tamilkodi R, Nesakumari GR (2021) A novel framework for retrieval of image using weighted edge matching algorithm. Multimed Tools Appl 80:19625–19648
20. Srinivasa Rao P, Yedukondalu K, Ganesh R (2021) FPGA implementation of digital 3-D image skeletonization algorithm for shape matching applications. Int J Electron 108:1326–1339
21. Lu B, Sun L, Yu L, Dong X (2021) An improved graph cut algorithm in stereo matching. Displays 69:102052

22. Nie M, Pan C, Wang J, Cai C (2021) A hybrid 3D particle matching algorithm based on ant colony optimization. Exp Fluids 62:1–17
23. Wang Z, Feng X, Wu Y et al (2021) An automatic method for matching salient structures in optical remote sensing images. Int J Remote Sens 42:8298–8317
24. Shao F, Liu Z, An J (2021) Feature matching based on minimum relative motion entropy for image registration. IEEE Trans Geosci Remote Sens 60:1–12
25. Xiang Z, Zhou G, Zhou Y, Luo Q (2022) Golden sine cosine salp swarm algorithm for shape matching using atomic potential function. Expert Syst 39:e12854
26. Rosenke C, Liśkiewicz M (2020) The generic combinatorial algorithm for image matching with classes of projective transformations. Inf Comput 275:104550
27. Liu F (2019) 3D block matching algorithm in concealed image recognition and E-commerce customer segmentation. IEEE Sens J 20:11761–11769
28. Shao W, Cao L, Guo W et al (2020) Visual navigation algorithm based on line geomorphic feature matching for Mars landing. Acta Astronaut 173:383–391
29. Shen J, Tao D, Li X (2008) Modality mixture projections for semantic video event detection. IEEE Trans Circuits Syst Video Technol 18:1587–1596
30. Liu D, Wu L, Hong R et al (2023) Generative metric learning for adversarially robust open-world person re-identification. ACM Trans Multimed Comput Commun Appl 19:1–19
31. Chopra N, Ansari MM (2022) Golden jackal optimization: A novel nature-inspired optimizer for engineering applications. Expert Syst Appl 198:116924
32. Luo Q, Li J, Zhou Y (2019) Spotted hyena optimizer with lateral inhibition for image matching. Multimed Tools Appl 78:34277–34296
33. Rosner B, Glynn RJ, Ting Lee M-L (2003) Incorporation of clustering effects for the Wilcoxon rank sum test: a large-sample approach. Biometrics 59:1089–1098